ADVANCED ELECTRONIC MATERIALS
www.advelectronicmat.de

Implantable Organic Artificial Synapses Exhibiting Crossover between Depressive and Facilitative Plasticity Response

Gioacchino Calandra Sebastianella, Michele Di Lauro, Mauro Murgia, Michele Bianchi, Stefano Carli, Michele Zoli, Luciano Fadiga, and Fabio Biscarini*

Organic neuromorphic devices mimic signal processing features of biological synapses, with short-term plasticity, STP, modulated by the frequency of the input voltage pulses. Here, an artificial synapse, made of intracortical microelectrodes, is demonstrated that exhibits either depressive or facilitative STP. The crossover between the two STP regimes is controlled by the frequency of the input voltage. STP features are described with an equivalent circuit where an inductance component is introduced in parallel with the RC circuit associated with poly(3,4-ethylenedioxythiophene)/polystyrene sulfonate (PEDOT/PSS)||electrolyte interface. The proposed RLC circuit explains the physical origin of the observed STP and its two timescales in terms of charge build up in PEDOT/PSS.

1. Introduction

Neuromorphic electronics pursues the development of device architectures whose response depends on the previous history of the device, mimicking some processing functions of the brain in comparison, classification, and memory storage.[1] Since the first reports of neuromorphic behavior in electronics,[2,3] a significant effort has been devoted to develop computing architectures based on such devices, with the aim to approach the computational and energetic efficiency of the human brain.[4] In neural (and neuromorphic) architectures, computation and data storage occur in the same physical space, overcoming the so-called "Von Neumann bottleneck."[5] Within this context, organic conductors and semi-conductors have been proposed as active materials for neuromorphic applications, giving rise to the field of organic neuromorphic electronics.[6,7] Such materials behave as organic mixed ionic–electronic conductors—OMIECs,[8] whose time response is dictated by the dynamic interplay between ions (slow carriers) and electrons (fast carriers) as well as the features of input signals. OMIECs are operated in aqueous environment and under driving voltages that are within the electrochemical stability window of water, which make them candidate for interfacing the living matter.[9–11] These features make OMIECs attractive for neuromorphic devices especially in comparison to silicon-based devices.[12]

The first report of neuromorphic behavior in organic electronic devices was achieved by the NOMFET (nanoparticle organic memory field effect transistor) architecture.[13] In NOMFET, the slow kinetic phenomenon necessary to elicit a neuromorphic response was obtained by embedding gold nanoparticles that act as shallow traps in an organic semiconductor thin film. In an aqueous environment, the slow kinetics is inherent to the ion displacement in the electrolyte at the interface with the active OMIEC. A number of neuromorphic devices were demonstrated in aqueous electrolytes, from switchable nonvolatile memory elements[14] to devices emulating the main synaptic signal processing features, like spike-timing-dependent-plasticity,[15,16] short-term-plasticity (STP),[17,18] and long-term-potentiation.[7,19–21] These functions are the basis of processing, memorization, and learning mechanisms in the human brain.[22] Recently, such architectures were integrated with cultured neural cells with neither loss of functionality nor impairment of cell viability,[23] leading to the demonstration of the first bio-hybrid synapses.[24]

The sensitivity of neuromorphic synapses to the composition of the ionic environment arises from the interplay of dynamic noncovalent interactions between molecular solutes and OMIEC, which establishes the timescale of the neuromorphic

G. Calandra Sebastianella, M. Zoli
Dipartimento di Scienze Biomediche
Metaboliche e Neuroscienze
Università di Modena e Reggio Emilia
Via Campi 287, Modena 41125, Italy

M. Di Lauro, M. Murgia, M. Bianchi, S. Carli, L. Fadiga, F. Biscarini
Center for Translational Neurophysiology of Speech and Communication
Fondazione Istituto Italiano di Tecnologia (IIT-CTNSC)
via Fossato di Mortara 19, Ferrara 44121, Italy
E-mail: michele.dilauro@iit.it

M. Murgia
Istituto per lo Studio dei Materiali Nanostrutturati (CNR-ISMN)
National Research Council
Via P. Gobetti 101, Bologna 40129, Italy

L. Fadiga
Sezione di Fisiologia
Dipartimento di Neuroscienze e Riabilitazione
Università di Ferrara
via Fossato di Mortara 17, Ferrara 44121, Italy

F. Biscarini
Dipartimento di Scienze della Vita
Università di Modena e Reggio Emilia
Via Campi 103, Modena 41125, Italy

The ORCID identification number(s) for the author(s) of this article can be found under https://doi.org/10.1002/aelm.202100755.

DOI: 10.1002/aelm.202100755

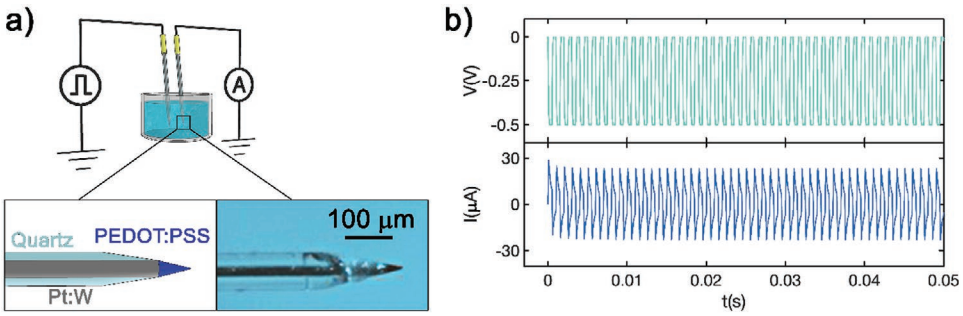

Figure 1. a) Schematic representation of the proposed implantable artificial synapse. Inset: schematics and optical micrograph of the tip; b) Example of current depressive response (bottom, dark blue) at the post-synaptic electrode, achieved pulsing the pre-synaptic electrode with a 1 kHz voltage square wave (top, light green).

response. This suggested the use of organic neuromorphic devices as sensors for species that exhibit an interaction with OMIEC stronger than that with ions in the electrolyte. This can be done even without endowing them with specific bio-recognition groups, such as enzymes,[25] antibodies,[26] or aptamers.[27] This feature was used to discriminate dopamine (a cation at physiological pH) not only from its antagonists in electrochemical assays[28] but also from its metabolites and catabolites[29] where the only difference is a single substitution. Quantification of the relevant molecule is inferred from the change of the time constant of depressive STP elicited in an OMIEC-based artificial synapse upon a 500 Hz stimulation. Translating this proof-of-concept to in vivo would be important for in situ real-time detection of dopamine that may in perspective open the way to loco-regional treatments of neurodegenerative conditions like Parkinson's disease.

Toward this aim, we have endowed deep-brain fiber microelectrodes,[30] originally designed for stimulation and recording, with neuromorphic response by electrochemically coating their tips with poly(3,4-ethylenedioxythiophene)/polystyrene sulfonate—PEDOT/PSS. This coating is usually aimed at reducing interface impedance and/or at increasing biocompatibility in neural applications.[31–35] Here, a further function, viz., ability to exhibit STP, is demonstrated. In this investigation, the input frequency is systematically varied across two orders of magnitude, unveiling a crossover from depressive (at high frequency input voltage pulses) to facilitative (at lower frequency input voltage pulses) STP responses. An equivalent circuit model is then proposed to rationalize the observed STP response, which shows how the introduction of an inductive component in parallel with the usual RC circuit adopted for purely depressive STP, allows one to fit and predict the observed STP signals and their crossover. For the first time, the inductance is used for explaining the neuromorphic response in OMIEC-based artificial synapses, which points to the role of charge build up inside the OMIEC as an ionic mechanism of control of the STP features.

2. Results and Discussion

2.1. System Design and Characterization

The proposed architecture and its connection layout are shown in **Figure 1**a. As discussed above, the electrochemical deposition of PEDOT/PSS (blue film in the schematic drawing) yields a significant reduction of the impedance $|Z|$ in comparison to the bare Pt:W microelectrode. The electrode to the left acts as pre-synaptic terminal and is pulsed at a given frequency as it is connected to a square wave voltage source; the current response is recorded at the post-synaptic electrode to the right. Wave frequency is systematically halved from 2 kHz to 31.25 Hz, resulting in seven investigated frequency values (2 kHz, 1 kHz, 500, 250, 125, 62.5, and 31.25 Hz). Figure 1b shows a representative depressive STP current response, elicited at 1 kHz.

2.2. Frequency-Dependent STP Response

Figure 2a reports a 3D overlay of the STP response at all the investigated frequencies. We notice that: i) at high frequencies the plasticity of artificial synapses exhibits a depressive behavior, ii) a decrease of the input frequency results in the noticeable reduction of the current amplitude coupled to a gradual loss of the depressive behavior; iii) at input frequencies below 250 Hz the STP response turns gradually into a facilitative one. Notice that the facilitative response exhibits always smaller amplitude with respect to the depressive one. It is possible to highlight these effects in Figure 2b, where current responses to the first ten voltage pulses are reported versus the dimensionless product of time and frequency, $t \cdot f$, and in Figure 2c, where the envelopes of STP maxima are normalized to the first current spike, $I(0)$ and shown versus the time interval from the stimulation starting time. Figure 2c emphasizes the crossover from the depressive to the facilitative behavior of STP from high to low input frequencies.

A physical rationale of this behavior can be formulated by focusing on the mechanistic origin of the depressive STP behavior. At high input frequencies (500 Hz $< f <$ 2 kHz) the current response is dominated by the capacitive displacement current arising in the electrolyte in response to a sudden potential variation at the pre-synaptic electrode. Since the current decays in a time span longer than the inverse of the pulse frequency, the system fails to relax in the time interval between two subsequent spikes and attains a new pseudo-equilibrium determined by the build-up of an effective over-potential at the electrode/electrolyte interface upon continuous stimulation.[29]

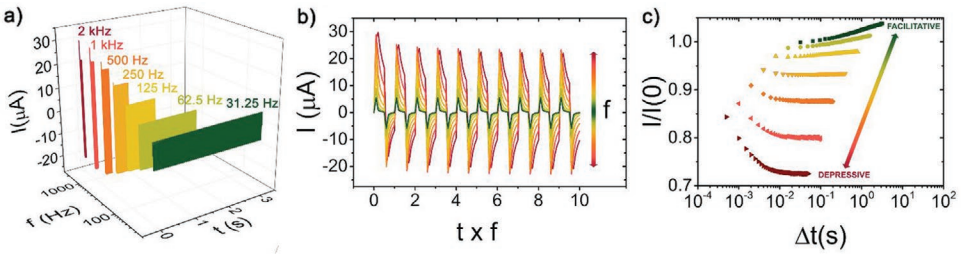

Figure 2. a) Current recorded at the post-synaptic terminal (*z*-axis) versus stimulation time (*x*-axis) and input voltage frequency (*y*-axis). b) Current recorded at the post-synaptic terminal versus the product of time and stimulation frequency (*x*-axis). The plot emphasizes amplitude decrease and loss of the depressive response as stimulation frequency decreases. c) Overlay of the normalized current envelopes $I/I(0)$ reported versus the time interval spanning from the first maximum to the time value of each maximum, reported in logarithmic scale.

2.3. Equivalent Circuit Model

The Randles equivalent circuit was suitable to describe the depressive STP response,[29] but it does not allow one to rationalize the emergency of the facilitative response and its amplitude decrease upon frequency decrease. Indeed, the Randles equivalent circuit exhibits a single frequency-independent RC time constant, which results in a *unique* frequency-independent STP depressive response. It is worth noticing that the rise time of the square pulses (i.e., the derivative of voltage in time) is independent from the chosen stimulation frequency and, accordingly, the displacement current in a Randles circuit would maintain its amplitude at all the input frequencies. In the present artificial synapse, instead, an amplitude decrease is observed in response to pulse frequency decrease.

Both these effects can be accounted for only by introducing a time/frequency-dependent resistive contribution which, in electrochemical systems, is represented by a "pseudo-inductance," as proposed by Gutmann.[36] Such a definition, which identifies the electrochemical pseudo-inductance as a "region of space capable of reversibly storing electric energy kinetically," accounts for the phenomenon at the origin of this varying resistive contribution, namely, the motion of ions that drift at the interface between PEDOT/PSS and electrolyte. This motion spans the entire volume of the PEDOT/PSS film and modulates its conductivity. Evidences of such pseudo-inductive behavior in PEDOT/PSS-based systems were reported in studies concerning to nonideal response of organic electrochemical transistors to both *I–V* characterization[37] and electrochemical impedance spectroscopy;[38] furthermore, pseudo-inductive behavior is widely explored in the context of energy storage devices.[39]

The equivalent circuit used to describe our organic artificial synapse is depicted in **Figure 3**. It involves a minimum modification of the Randles equivalent circuit by adding an inductive term at the PEDOT/PSS‖electrolyte interface. In detail, the proposed circuit features a solution resistance (R_E) in series with an RLC section constituted by the double layer resistance (R_{DL}), the double layer capacitance (C_{DL}), and the PEDOT/PSS film pseudo-inductance (L_F). A pulsed voltage source provides square wave stimulation and the amperometer (A) measures the overall output current.

It is possible to provide a quantitative description of the STP response by analytically solving the circuit in Figure 3.

The input periodic square wave in the Laplace domain reads

$$V(s) = \frac{V_0}{s\left(1+e^{-s\Theta T}\right)} \tag{1}$$

where V_0 is the amplitude, Θ is the duty cycle, T is the period—namely, the inverse of the stimulation frequency—, and s is the Laplace variable.

In the same domain, the impedances of the passive circuit elements are defined as $Z_{R_E}(s) = R_E$, $Z_{R_{DL}}(s) = R_{DL}$, $Z_{L_F}(s) = sL_F$, and $Z_{C_{DL}}(s) = \frac{1}{sC_{DL}}$. As a consequence, the overall circuit impedance reads as

$$Z(s) = R_E + \left(\frac{1}{R_{DL}} + \frac{1}{sL_F} + sC_{DL}\right)^{-1} \tag{2}$$

and, from Ohm's law, one obtains

$$I(s) = \frac{V(s)}{Z(s)} = \frac{V_0}{s\left(1+e^{-s\Theta T}\right)} \frac{1}{R_E + \left(\frac{1}{R_{DL}} + \frac{1}{sL_F} + sC_{DL}\right)^{-1}} \tag{3}$$

Equation (3) describes the current in the Laplace domain. Applying the inverse Laplace transform to Equation (3),

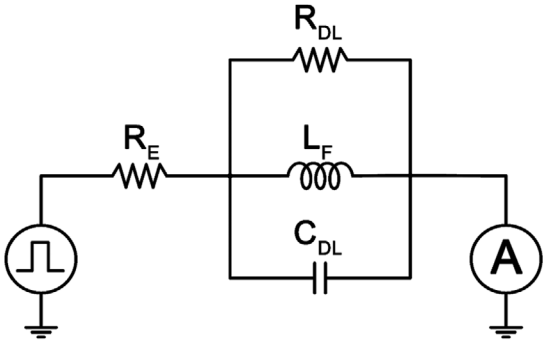

Figure 3. Equivalent circuit proposed to model our artificial synapse. It involves an RLC branch composed by the pseudo-inductance of the PEDOT/PSS film (L_F) in parallel with the double layer resistance (R_{DL}) and the double layer capacitance (C_{DL}). The RLC branch is in series with the electrolyte resistance (R_E).

Table 1. Expression of the coefficients in Equation (4).

Parameter	Expression	Units
R_{eff}	$\frac{R_{DL}R_E}{R_{DL}+R_E}$	Ω
τ	$C_{DL}R_{eff}$	s
η	$\frac{L_F}{R_{eff}}$	s
ρ	$\sqrt{1-4\frac{\tau}{\eta}}=\sqrt{1-4\frac{C_{DL}R_{eff}^2}{L_f}}$	–
Γ	$\frac{\rho-1}{2\tau}$	Hz
M	$\frac{\rho+1}{2\tau}$	Hz

$I(t)=\mathcal{L}^{-1}[I(s)]$, we obtain the current in the time domain, shown in Equation (4)

$$I(t)=\frac{V_0}{R_E}\left\{\left[\frac{1-(-1)^{\lfloor -t/\Theta T\rfloor}}{2}\right]+\frac{1}{\rho}\frac{R_{eff}}{R_E}\left[\frac{e^{-Mt}\left(1-\left(-e^{-M\Theta T}\right)^{\lfloor -t/\Theta T\rfloor}\right)}{1+e^{M\Theta T}}-\frac{e^{\Gamma t}\left(1-\left(-e^{\Gamma\Theta T}\right)^{\lfloor -t/\Theta T\rfloor}\right)}{1+e^{-\Gamma\Theta T}}\right]\right\} \quad (4)$$

where we grouped circuit elements in the coefficients listed in **Table 1**. $\lfloor x\rfloor$ is the floor function, which returns the greatest integer less than or equal to x.

Equation (4) is the analytical expression of the entire STP current profile and can be used to predict the neuromorphic response of an organic artificial synapses, provided that the values of all the equivalent circuit elements are known, else to fit the experimental STP with only four fitting parameters, e.g., R_{eff}, R_E, C_{DL}, L_F.

The observed trends can be explained by introducing the time constants τ and η, the former related to the capacitive response and the latter depending on the electrochemical pseudo-inductance. The time constants can be combined in the dimensionless parameter, ρ, which weights the contribution of τ to the two frequency constants, Γ and M, accounting for the facilitative and the depressive response, respectively.

We limit our discussion to the domain of real non-negative values for ρ, viz., $0 \le \rho \le 1$, and $\frac{\tau}{\eta}=\frac{C_{DL}R_{eff}^2}{L_f}<\frac{1}{4}$. This implies also that $-\frac{1}{2\tau}\le\Gamma\le 0$ and $\frac{1}{2\tau}\le M\le\frac{1}{\tau}$. In general, Γ is always nonpositive, and M is always positive.

Interestingly, $\rho = 1$ yields $\Gamma = 0$ and Equation (4) depends only on $=\frac{1}{\tau}$. This is the case in which L_F approaches infinite and the inductive contribution is negligible, exactly reproducing the behavior of purely depressive STP.[29]

We then derived the analytical expression for the discrete envelope of STP maxima, expressing the current as a function of the pulse number (n), instead of time (t). The pulse number, n, is an integer number ranging from 0 to N including the range boundaries, where N is the total number of administered pulses. The number n is obtained by subtracting 1 from the pulse number, e.g., for the first spike, $n = 0$.

The time values at which maxima are observed, t_M, can be expressed as a function of the time of the first spike, $t_{M,0}$ and of n, as $t_M(n) = t_{M,0}+nT$. In the proposed experimental conditions, where STP analysis starts one sample before the first voltage pulse, $t_{M,0}$ always corresponds to the sampling time, t_s, which is the inverse of the sampling frequency. The expression of the maxima time values as a function of n can be re-written as

$$t_M(n)=t_s+nT \quad (5)$$

At these time values, the exponential term $\lfloor -t/\Theta T\rfloor$ from Equation (4) can be re-written as

$$\left\lfloor -\frac{t_M}{\Theta T}\right\rfloor=-\left\lfloor\frac{(t_s+nT)}{\Theta T}\right\rfloor=\left\lfloor -\frac{t_s}{\Theta T}-\frac{n}{\Theta}\right\rfloor \quad (6)$$

In our experiment, where $\Theta = 1/2$, Equation (6) reads $\left\lfloor -\frac{2t_s}{T}-2n\right\rfloor=\left\lfloor -\frac{2t_s}{T}\right\rfloor-2n$, as follows from the peculiarities of the floor function, since $2n$ is always integer. In our setup, the sampling time t_s is one tenth of the period T, regardless of the investigated frequency, implying that $\left\lfloor -\frac{2t_s}{T}\right\rfloor=-1$. This can be extended to any STP experiment in which the sampling time is shorter than, or equal to, half of the period T: for $0<t_s\le\frac{T}{2}$ it will follow that $0<\frac{2t_s}{T}\le 1$.

Equation (4) is recast in its discrete form

$$I(n)=\frac{V_0}{R_E}\left\{1+\frac{1}{\rho}\frac{R_{eff}}{R_E}\left[\frac{e^{-Mt_s}\left(e^{-nMT}+e^{MT/2}\right)}{1+e^{MT/2}}-\frac{e^{\Gamma t_s}\left(e^{n\Gamma T}+e^{-\Gamma T/2}\right)}{1+e^{-\Gamma T/2}}\right]\right\} \quad (7)$$

because for any n value, $(-1)^{-1-2n} = -1$. Equation (7) can be further simplified obtaining Equation (8), which is the analytical expression of the STP envelope as a function of n

$$I(n)=\frac{V_0}{R_E}\left[\gamma+\alpha e^{-\frac{n}{\theta}}-\beta e^{-\frac{n}{\sigma}}\right] \quad (8)$$

where parameters from Equation (7) have been grouped as reported in **Table 2**.

Table 2. Parameters in Equation (8).

Parameter	Expression
α	$\frac{1}{\rho}\frac{R_{eff}}{R_E}\frac{e^{-Mt_s}}{1+e^{MT/2}}$
β	$\frac{1}{\rho}\frac{R_{eff}}{R_E}\frac{e^{\Gamma t_s}}{1+e^{-\Gamma T/2}}$
γ	$1+\alpha e^{1/2\theta}-\beta e^{1/2\sigma}$
θ	$\frac{1}{MT}$
σ	$-\frac{1}{\Gamma T}$

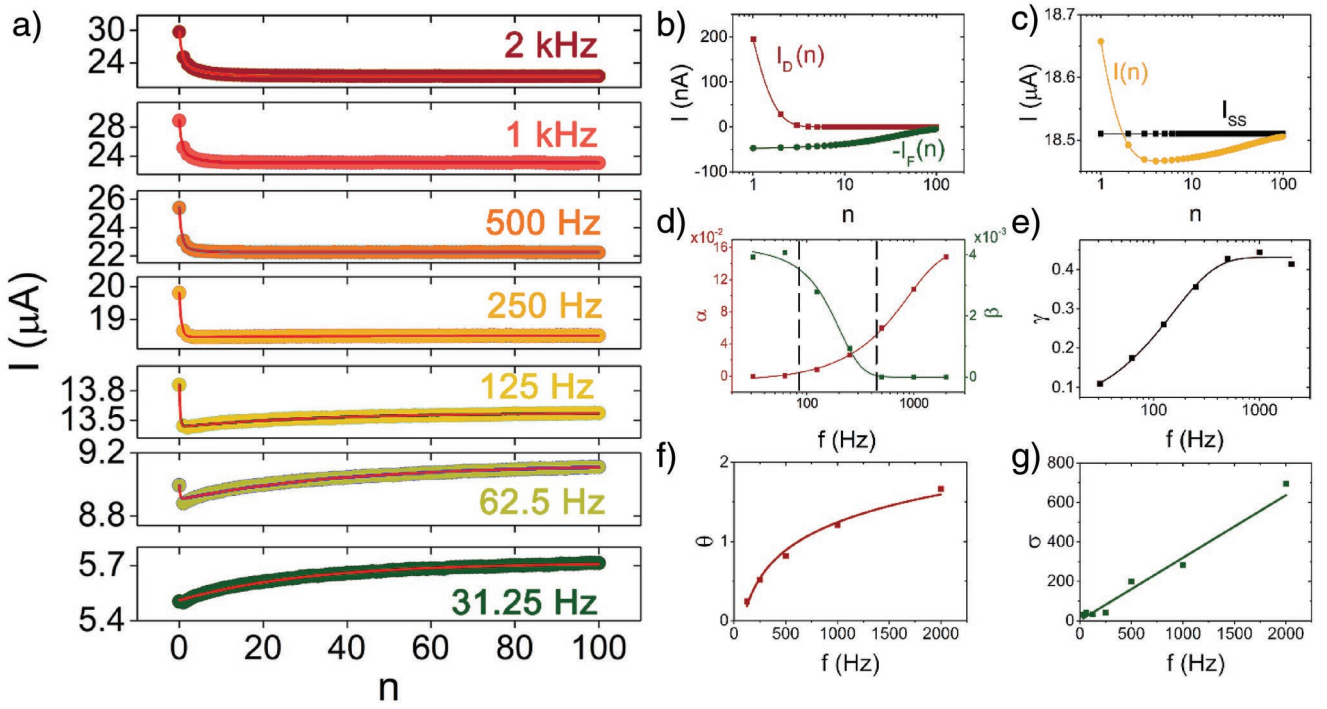

Figure 4. a) Envelopes of the maxima of the current response reported versus pulse number at all the investigated frequency values and fitted with Equation (9); b) log-lin plot of I_D and $-I_F$ versus pulse number, n, as calculated by fitting STP at 250 Hz with Equation (9); c) log-lin plot of constant steady-state current, I_{SS}, and full STP envelope, I, versus pulse number, n, as calculated by fitting STP at 250 Hz with Equation (9); d) log-lin overlay of the depressive weight, α, and the facilitative weight, β, as a function of frequency. It is possible to distinguish the three frequency regions where the system responds either in a purely depressive manner (high frequencies), in a purely facilitative one (low frequencies), or with a mixed behavior (crossover region); sigmoidal fits are guides for the eye; e) log-lin plot of the steady-state weight, γ, as a function of frequency, showing a high-pass behavior of the electrolyte. The sigmoidal fit is a guide for the eye; f) lin-lin plot of I_D decay constant, θ, as a function of frequency, with logarithmic fit; g) lin-lin plot of I_F decay constant, σ, as a function of frequency, with linear fit.

By fitting experimental data at each stimulation frequency, as shown in **Figure 4**a, it is possible to obtain descriptors of the STP behavior from Equation (8) where the STP envelope is expressed as the partition of the ohmic current in the electrolyte, V_0/R_E, among a steady-state term, whose weight is γ, and two additive depressive and facilitative terms, weighted by the pre-exponential weights α and β, respectively. The latter two decay versus n with decay constants, σ and θ, both positive. Thus, when n exceeds either σ and/or θ, the facilitative STP contribution and/or the depressive STP contribution disappear, respectively. Owing to the fact that $|M| > |I|$, then $\sigma > \theta$ meaning that the depressive STP will be always faster than the facilitative STP, and will disappear within lesser number of pulses.

The overall current response is hence contributed by three terms shown in Equation (9)

$$I(n) = I_{SS} + I_D(n) - I_F(n) \tag{9}$$

where $I_{SS} = \frac{\gamma V_0}{R_E}$ is the steady-state current, $I_D(n) = \frac{V_0}{R_E}\alpha e^{-\frac{n}{\theta}}$ is a fast-decaying additive contribution to the current which accounts for the depressive STP and $I_F(n) = \frac{V_0}{R_E}\beta e^{-\frac{n}{\sigma}}$ is a slow-decaying subtractive contribution which accounts for the facilitative response. To highlight the role of the weighted current contributions, the depressive, $I_D(n)$, and facilitative, $I_F(n)$, contributions to the STP at 250 Hz response are reported in Figure 4b. They both converge to zero plateau value, with different dynamics the slowest, else the one requiring greater number of pulses n, being the facilitative one. Figure 4c shows the constant steady-state current, I_{SS}, and the total current $I(n)$, as obtained from Equation (9). As predicted by Equation (8), the value of the first maximum, $I(0) = \frac{V_0(\alpha - \beta + \gamma)}{R_E}$ and, since both the exponential terms in Equation (8) feature negative exponents, the influence of I_D and I_F in determining the value of $I(n)$ decreases as n increases. The number of pulses which is required for damping each contribution is quantitatively expressed by θ and σ, viz., $n > \theta$ and $n > \sigma$, respectively. This is commented at the end of this section.

By extracting R_E by electrochemical impedance spectroscopy, it is possible to obtain the values of the weights α, β, and γ and of the decay constants θ and σ upon fitting of the envelopes. We fit the experimental envelopes and show the trends of the parameters versus frequency in Figure 4d–g. This allows us to rationalize the observed crossover from facilitative to depressive behavior upon frequency increasing.

The pre-exponential terms, α and β, exhibit opposite trends versus frequency, as shown in Figure 4d, with α increasing and β decreasing upon frequency increase. Three frequency ranges are identified among which artificial synapses show different STP responses: at low frequencies (<100 Hz), $\alpha \approx 0$, hence

$I(n) \approx I_{SS} - I_F(n)$. The net facilitative effect observed results from the exponential decay of $I_F(n)$ for increasing n

$$I(\infty) = I_{SS} > I(0) \approx I_{SS} - I_F(0) \tag{10}$$

This effect is progressively lost upon frequency increase/period decrease since, as discussed above, the pseudo-inductive contribution becomes negligible. Indeed, at higher frequencies (≥500 Hz), $\Gamma = 0$, $\sigma = +\infty$, $L_F \to +\infty$, $\rho = 1$, leading to $I_F = 0$. Thus, in the absence of inductive contributions, only depressive mono-exponential STP decay can be elicited and Equation (8) becomes[17,29,37,38]

$$I(n) = \frac{V_0}{R_E}\left[1 + \frac{R_{eff}}{R_E}\left[\frac{e^{-Mt_s}}{1+e^{MT/2}}\left(e^{-\frac{n}{\theta}} + e^{\frac{1}{2\theta}}\right) - 1\right]\right] \tag{11}$$

In the intermediate frequency range (from 100 to 500 Hz), around 250 Hz, the facilitative and depressive regimes are co-existing, and a mixed behavior characterized by fast depression and slow facilitation is observed. It must be noticed that the variability range of the depressive weight, α, is one order of magnitude larger than that of the facilitative weight, β; hence, in the facilitative region, the amplitude is more-than-tenfold lower than the amplitude of the depression in the depressive region. This confirms the experimental observation in Figure 4a.

The I_D decay constant of the depressive term, θ (Figure 4g) accounts for the depressive contribution and increases with the logarithm of the square root of frequency. The I_D decay constant, σ (Figure 4f) diverges approaching infinite with a linear dependence on frequency, which accounts for the electrochemical pseudo-inductance representing the kinetic storage of electrostatic energy. This is allowed at low frequency and prohibited at high frequencies. These trends are coherent with the definitions of θ and σ (see Table 2), which depend on M^{-1} and Γ^{-1}, and the period of stimulation T, respectively.

In summary, our model predicts the following regimes as a function of the number of pulses supplied, and interestingly, depending on the period T (equivalently its frequency $1/T$), or, more precisely, the ratio T/τ:

1) $n >> \sigma > \theta$ plateau;
2) $n < \sigma$ and $n >> \theta$ facilitative STP, not depressive STP;
3) $n < \theta < \sigma$ facilitative STP and depressive STP coexist. The weights α and β determine which STP behavior dominates. Since $\alpha >> \beta$ at high frequencies, hence depressive STP dominates; vice versa $\alpha < \beta$ at low frequencies makes facilitative STP to dominate.
4) $n < \theta << \sigma$ depressive STP, not facilitative STP. This implies that $MT >> -\Gamma T$, and hence $\rho T/\tau >> 0$. The maximum depressive STP is observed for $\rho = 1$ and $T >> \tau$. This is the situation where, de facto, one applies single pulses, largely spaced, so the system does not retain memory of the previous ones. On this particular case, somewhat counterintuitively, the very slow input wave yields a depressive STP.

From the operation point of view, especially to obtain devices with targeted response, our model appears useful for estimating how many pulses are actually needed for inducing a depressive STP and/or facilitative STP.

3. Conclusions

We presented an implantable artificial synapse made of two intracortical microelectrodes whose tips are coated by electrodeposited PEDOT/PSS films. A systematic investigation of the STP response of such architecture was performed varying the pre-synaptic frequency over two decades. A transition from facilitative to depressive STP behavior upon frequency increase is observed. We explain this transition and the coexistence of both depressive and facilitative behaviors by the modulation of a frequency-dependent inductive contribution in parallel to the equivalent circuit model commonly used for describing the depressive STP. Laplace analysis of the equivalent circuit allowed us to reproduce the STP current trends versus time and to discretize the envelope of the current maxima versus the number of input voltage pulses, thus providing a set of quantitative descriptors of neuromorphic response of such devices.

We highlight here the novel and important results for organic neuromorphic devices: i) at a given frequency, STP manifests itself either as depressive or facilitative, else as a coexistence of the two regimes; ii) the input frequency determines what of the three regimes is the dominant one; thus, in principle, even a "pure" frequency input to an organic neuromorphic device that was not conditioned before (then, does not retain memory of its previous history), allows one to instruct the system to respond in one of the three modes; iii) the coexistence of the depressive and facilitative regimes, the former with faster and the second with slower timescales, is, in reality, the "unifying" or "universal" regime. The number of input voltage pulses determines whether we observe only depressive (one needs many more pulses for the system to turn into facilitative STP at high frequencies), facilitative (depressive is only for a few pulses at the onset of stimulation at low frequencies), or both. The number of pulses is, therefore, an independent control of the STP response that the system outputs, iv) the amplitude of STP is another valuable information about the input signal, as we noticed that high frequency tends to maintain the amplitude of the response, whereas at low frequencies we observe a net lowering of the amplitude. It turns out that information flow is coded not only in the timescales but also on the STP amplitudes.

Another relevant result is that we have been able to link the timescales and their interplay to the presence of a simple, albeit new, element in the equivalent circuit, viz., the electrochemical pseudo-inductance, that accounts to some extent on the ion gradient created inside the active material (PEDOT/PSS in our case) and that progressively builds up an internal potential against ion diffusion across the volume, as confirmed by the scaling of pseudo-inductive behavior in organic electronic devices with electrolyte ion concentration[38] and by other evidence that we reported recently, namely, the saturation of effective capacitance and electroactive area versus the volume of the active layer.[40] The novelty of these aspects should stimulate research toward ways of controlling, or finely tuning, the inductance element in the framework of RLC circuits. This is an intriguing finding,

since most of the previous reports addressed depressive STP and related its timescale to an RC equivalent circuit. It was also observed the emergence of facilitative response when higher frequency stimulation (driving the system into depressive STP) is followed by a low frequency stimulation. However, this is the first time to our knowledge, where the crossover between the two regimes is clearly demonstrated to occur also within a constant frequency stimulation, and how this coincides with the inductance taking a finite value.

Finally, the importance of this work from an electrophysiology point of view is that demonstrates the fabrication and proof-of-concept operation of implantable artificial synapses. As simple as the architecture may appear, it is a change of paradigm in electrophysiology as it would become possible to design components and circuitry with targeted response to specific physiologically relevant frequency patterns. This is an attractive feature, as it will move the frontiers of (passive) electrophysiological recording to devices able to recognize specific signals related to a given pathology or to transient deficits. These characteristics, together with the advantages of organic neuromorphic devices in terms of biocompatibility and power consumption, are worth to be explored, in view of developing standalone therapeutic devices, able to monitor electrical and/or chemical signals, and react accordingly when the monitored features match those of the target signal, for instance by controlling local drug delivery or administering a voltage stimulus.

We believe that methodological and analytical tools herein provided widen the applicability range of organic artificial synapses, enabling tunable STP for sensing and signal processing in in vivo applications. This will be at the basis of next-generation locoregional therapy with implanted devices for neurological disorders like drug-resistant epilepsy or Parkinson's disease.

4. Experimental Section

Artificial Synapse Fabrication: The proposed synaptic architecture involved two fiber electrodes (Thomas RECORDING GmbH) immersed in an electrolyte at a fixed distance of 1 mm. Each fiber electrode was composed by a metal core (Pt:W, 95:5) with a diameter of 25 µm, surrounded by a quartz insulating layer, for an overall diameter of 80 µm.

PEDOT/PSS Electrodeposition: PEDOT/PSS electrodeposition was carried out, according to published protocols,[41–43] from an aqueous solution of EDOT (3,4-Ethylenedioxythiophene, 10×10^{-3} M) and NaPSS (sodium polystyrene sulfonate, 0.7% w/w) in potentiostatic mode (1 V vs Ag|AgCl; 5 s pre-conditioning step: 0.2 V vs Ag|AgCl). A three-electrode cell setup was achieved using a titanium sheet as the counter electrode, a Ag|AgCl (3 M KCl_{aq}) as the reference electrode and the fiber electrode as the working electrode, using a Gamry Reference 600 potentiostat/galvanostat (Gamry Instruments). The deposition was carried out under charge control and terminated upon exchanging a total charge of 2.5 µC, that corresponded to a charge density of roughly 125 mC cm^{-2} (tip lateral surface $\approx 2 \times 10^{-5}$ cm^2). Before and after electrodeposition of PEDOT/PSS, electrodes were characterized by means of electrochemical impedance spectroscopy.

Neuromorphic Response Characterization: STP was assessed in a 100×10^{-3} M phosphate-buffered saline solution using a two channel Keysight B2912A source-measure unit in a Faraday cage. Low-force terminals of both channels were connected to ground. High-force terminals of channel 1 and channel 2 were connected to the pre-synaptic and post-synaptic electrodes, respectively. Channel 1 was used as a voltage source to pulse the voltage of the pre-synaptic terminal between 0 and –0.5 V, with a 50% duty cycle; channel 2, used as an amperometer, recorded the resulting current at the post-synaptic terminal with a sampling frequency ten times higher than the stimulus frequency, thus keeping constant the number of samples throughout all the experiments (i.e., 10 samples per period).

Acknowledgements

L.F. and F.B. contributed equally to this work. Research work leading to this publication was funded by the IIT-Italian Institute of Technology, University of Ferrara, University of Modena and Reggio Emilia (FAR 2018 E-MAP and MIUR, Italy "Dipartimenti di eccellenza 2018–2022").

Open Access Funding provided by Istituto Italiano di Tecnologia within the CRUI-CARE Agreement.

Conflict of Interest

The authors declare no conflict of interest.

Data Availability Statement

Research data are not shared.

Keywords

artificial synapses, implantable electronics, neuromorphic device modeling, organic neuromorphic devices, short-term plasticity

Received: July 26, 2021
Revised: September 2, 2021
Published online: October 20, 2021

[1] D. Marković, A. Mizrahi, D. Querlioz, J. Grollier, *Nat. Rev. Phys.* **2020**, *2*, 499.
[2] C. Mead, *Proc. IEEE* **1990**, *78*, 1629.
[3] M. Carver, M. Ismail, *Analog VLSI Implementation of Neural Systems*, Kluwer Academic Publishers, Boston/Dordrecht/London **1989**.
[4] M. D. McDonnell, K. Boahen, A. Ijspeert, T. J. Sejnowski, *Proc. IEEE* **2014**, *102*, 646.
[5] P. Pacheco, *An Introduction to Parallel Programming*, Morgan Kaufmann, Burlington, MA **2011**.
[6] Y. Tuchman, T. N. Mangoma, P. Gkoupidenis, Y. Van De Burgt, R. A. John, N. Mathews, S. E. Shaheen, R. Daly, G. G. Malliaras, A. Salleo, *MRS Bull.* **2020**, *45*, 619.
[7] Y. Van De Burgt, A. Melianas, S. T. Keene, G. Malliaras, A. Salleo, *Nat. Electron.* **2018**, *1*, 386.
[8] B. D. Paulsen, K. Tybrandt, E. Stavrinidou, J. Rivnay, *Nat. Mater.* **2019**, *19*, 13.
[9] S. Inal, J. Rivnay, A. O. Suiu, G. G. Malliaras, I. McCulloch, *Acc. Chem. Res.* **2018**, *51*, 1368.
[10] T. Someya, Z. Bao, G. G. Malliaras, *Nature* **2016**, *540*, 379.
[11] D. T. Simon, E. O. Gabrielsson, K. Tybrandt, M. Berggren, *Chem. Rev.* **2016**, *116*, 13009.
[12] Y. Lee, T. W. Lee, *Acc. Chem. Res.* **2019**, *52*, 964.
[13] F. Alibart, S. Pieutin, D. Guérin, C. Novembre, S. Lenfant, K. Lmimouni, C. Gamrat, D. Vuillaume, *Adv. Funct. Mater.* **2010**, *20*, 330.
[14] Y. Van De Burgt, E. Lubberman, E. J. Fuller, S. T. Keene, G. C. Faria, S. Agarwal, M. J. Marinella, A. Alec Talin, A. Salleo, *Nat. Mater.* **2017**, *16*, 414.
[15] D. A. Lapkin, A. V. Emelyanov, V. A. Demin, T. S. Berzina, V. V. Erokhin, *Microelectron. Eng.* **2018**, *185–186*, 43.
[16] Q. Lai, L. Zhang, Z. Li, W. F. Stickle, R. S. Williams, Y. Chen, *Adv. Mater.* **2010**, *22*, 2448.

[17] Y. Hu, F. Zeng, C. Chang, W. Dong, X. Li, F. Pan, G. Li, *ACS Omega* **2017**, *2*, 746.
[18] M. Di Lauro, A. De Salvo, G. C. Sebastianella, M. Bianchi, S. Carli, M. Murgia, L. Fadiga, F. Biscarini, *ACS Appl. Electron. Mater.* **2020**, *2*, 1849.
[19] T. Chang, S. H. Jo, W. Lu, *ACS Nano* **2011**, *5*, 7669.
[20] Z. Wang, S. Joshi, S. E. Savel'ev, H. Jiang, R. Midya, P. Lin, M. Hu, N. Ge, J. P. Strachan, Z. Li, Q. Wu, M. Barnell, G. L. Li, H. L. Xin, R. S. Williams, Q. Xia, J. J. Yang, *Nat. Mater.* **2017**, *16*, 101.
[21] G. Liu, C. Wang, W. Zhang, L. Pan, C. Zhang, X. Yang, F. Fan, Y. Chen, R. W. Li, *Adv. Electron. Mater.* **2016**, *2*, 1500298.
[22] A. Volianskis, G. L. Collingridge, M. S. Jensen, *PeerJ* **2013**, *1*, e3.
[23] S. Desbief, M. di Lauro, S. Casalini, D. Guerin, S. Tortorella, M. Barbalinardo, A. Kyndiah, M. Murgia, T. Cramer, F. Biscarini, D. Vuillaume, *Org. Electron.* **2016**, *38*, 21.
[24] S. T. Keene, C. Lubrano, S. Kazemzadeh, A. Melianas, Y. Tuchman, G. Polino, P. Scognamiglio, L. Cinà, A. Salleo, Y. van de Burgt, F. Santoro, *Nat. Mater.* **2020**, *19*, 969.
[25] M. Berto, C. Diacci, L. Theuer, M. Di Lauro, D. T. Simon, M. Berggren, F. Biscarini, V. Beni, C. A. Bortolotti, *Flexible Printed Electron.* **2018**, *3*, 024001.
[26] M. Berto, S. Casalini, M. Di Lauro, S. L. Marasso, M. Cocuzza, D. Perrone, M. Pinti, A. Cossarizza, C. F. Pirri, D. T. Simon, M. Berggren, F. Zerbetto, C. A. Bortolotti, F. Biscarini, *Anal. Chem.* **2016**, *88*, 12330.
[27] M. Berto, C. Diacci, R. D'Agata, M. Pinti, E. Bianchini, M. Di Lauro, S. Casalini, A. Cossarizza, M. Berggren, D. Simon, G. Spoto, F. Biscarini, C. A. Bortolotti, *Adv. Biosyst.* **2017**, *2*, 1700072.
[28] M. Giordani, M. Berto, M. Di Lauro, C. A. Bortolotti, M. Zoli, F. Biscarini, *ACS Sens.* **2017**, *2*, 1756.
[29] M. Giordani, M. Sensi, M. Berto, M. Di Lauro, C. A. Bortolotti, H. L. Gomes, M. Zoli, F. Zerbetto, L. Fadiga, F. Biscarini, *Adv. Funct. Mater.* **2020**, *30*, 2002141.
[30] H. J. Reitboeck, *J. Neurosci. Methods* **1983**, *8*, 249.
[31] S. De Faveri, E. Maggioiini, E. Miele, F. De Angeiis, F. Cesca, F. Benfenati, L. Fadiga, *Front. Neuroeng.* **2014**, *7*, 7.
[32] S. M. Richardson-Burns, J. L. Hendricks, D. C. Martin, *J. Neural Eng.* **2007**, *4*, L6.
[33] D. H. Kim, J. A. Wiler, D. J. Anderson, D. R. Kipke, D. C. Martin, *Acta Biomater.* **2010**, *6*, 57.
[34] A. Ansaldo, E. Castagnola, E. Maggiolini, L. Fadiga, D. Ricci, *ACS Nano* **2011**, *5*, 2206.
[35] G. Baranauskas, E. Maggiolini, E. Castagnola, A. Ansaldo, A. Mazzoni, G. N. Angotzi, A. Vato, D. Ricci, S. Panzeri, L. Fadiga, *J. Neural Eng.* **2011**, *8*, 066013.
[36] F. Gutmann, *J. Electrochem. Soc.* **1965**, *112*, 94.
[37] D. Tu, R. Forchheimer, *Solid–State Electron.* **2012**, *69*, 7.
[38] S. Pecqueur, I. Lončarić, V. Zlatić, D. Vuillaume, Ž. Crljen, *Org. Electron.* **2019**, *71*, 14.
[39] C. Breitkopf, K. Swider-Lyons, *Springer Handbook of Electrochemical Energy*, Springer, New York **2016**.
[40] M. Bianchi, S. Carli, M. Di Lauro, M. Prato, M. Murgia, L. Fadiga, F. Biscarini, *J. Mater. Chem. C* **2020**, *8*, 11252.
[41] S. Carli, M. Bianchi, E. Zucchini, M. Di Lauro, M. Prato, M. Murgia, L. Fadiga, F. Biscarini, *Adv. Healthcare Mater.* **2019**, *8*, 1900765.
[42] M. Vomero, E. Castagnola, F. Ciarpella, E. Maggiolini, N. Goshi, E. Zucchini, S. Carli, L. Fadiga, S. Kassegne, D. Ricci, *Sci. Rep.* **2017**, *7*, 40332.
[43] C. Boehler, F. Oberueber, S. Schlabach, T. Stieglitz, M. Asplund, *ACS Appl. Mater. Interfaces* **2017**, *9*, 189.